Energy Conversion and Management 87 (2014) 495–503

Contents lists available at ScienceDirect

Energy Conversion and Management

journal homepage: www.elsevier.com/locate/enconman

Optimization of a thermoelectric system for power generation realized by "hidden" components

Maria La Gennusa, Massimo Morale, Gianluca Scaccianoce *

Dipartimento di Energia, Ingegneria dell'Informazione e Modelli Matematici, Università degli Studi di Palermo, Viale delle Scienze 9, Palermo, Italy

ARTICLE INFO

Article history:
Received 21 November 2013
Accepted 10 July 2014
Available online 3 August 2014

Keywords:
Thermoelectric effect
Solar thermal collector
Peltier cell

ABSTRACT

Today the utilization of renewable energy sources is very important to support the traditional ones, and also in order to reach the objectives fixed by the Kyoto Protocol.

In this context, also well-known technologies related to the electric energy production, formerly not suitable – due to the poor technological level of the components or due to the high costs linked to the system efficiency – may now find a suitable collocation.

Among these technologies, the thermoelectric effect may be very advantageous in some particular applications of small power. A power generation system utilizing this technology has been studied by the authors. This system utilizes the thermal difference between a lower temperature sink, e.g. a water reservoir, and a higher temperature source, such as exhaust heat (e.g. from industrial processes) or as produced by solar energy captured by an extended surface. The thermoelectric generator is made up of thermocouples placed on the internal surface of a tubular heat exchanger, located inside the water body and filled up with hot water coming from the energy source.

In this paper, the physical mechanisms and the energy balances governing the system are described in order to evaluate its energetic feasibility. Once fixed, the electrical power required by the end user, the system parameters are optimized with the aim to have the most compact equipment and components. A simulation of the proposed system was performed referring to the city of Palermo, Italy. A very poor economic convenience of the system has been found in this applications.

1. Introduction

A greater sensitiveness in public opinion towards environmental problems, highlighted by the media, especially in the more economically developed countries, joined with an increasing mean cost of fossil fuels, results in a more intensive utilization of renewable energy. This is also to reach the objectives signed by countries in the Kyoto protocol [28].

In the wide range of renewable energies in order to supply electrical energy, Research and Development look, with a new interest at techniques previously well-known but practically not implemented due to their low efficiencies, related either to the technological level of components, or to the unreasonable costs. Among these techniques there is the thermoelectric effect, characterized by low efficiencies but, in some particular applications, suitable to give good advantages: e.g. in small electric power applications where a regular electric supply is not suitable.

The thermoelectric elements, or thermocouples, exploit the principle observed by the German scientist Thomas Johann Seebeck in 1821 and, separately, observed by the French scientist Jean Charles Athanase Peltier in 1834. In a circuit made of two different metals by placing the junctions at two different temperatures, an electromotive force is generated. Vice versa by applying an electromotive force, it is possible to have different temperatures at the junctions and so a heat exchange. This effect is widely used in many engineering applications; it is the basic principle for a very easy to use, reliable and versatile temperature measuring system [23].

The system analyzed in this study [16] uses the thermal difference between a reservoir at a low temperature (e.g. groundwater, river), and a reservoir at a high temperature (e.g. waste heat in an industrial process, heat captured by a solar collector).

The system was previously designed to be used as an aid for the development of African villages, where an electrical supply was not available. The system components may be considered "hidden" because the heat exchanger at a high temperature may be placed on a roof (solar collector) or under the ground. The other heat exchanger at a low temperature must be dipped in a water

* Corresponding author. Tel.: +39 091 238 619 34; fax: +39 091 48 44 25.
E-mail address: gianluca.scaccianoce@unipa.it (G. Scaccianoce).

http://dx.doi.org/10.1016/j.enconman.2014.07.035
0196-8904/

Nomenclature

Latin symbols

A_c	overall surface area of solar collectors, m^2
C_{HW}	Hazen–Williams coefficient
c_p	specific heat at constant pressure, J kg^{-1} K^{-1}
D	diameter, m
d	thickness, m
d_{glass}	thickness of single cover
E	ends potential difference, V
F', F_R	solar collector factors
h	convective heat transfer coefficient, W m^{-2} K^{-1}
I	irradiance, W m^{-2}
K_{glass}	extinction coefficient of glass, m^{-1}
l, L	length, m
M	mass flow rate, kg/s
m	solar collector useful parameter
N	number of cover of solar collector
n	thermocouple density or cover refractive index
P	power, W
P_w	pump power, W
p	pressure, Pa
R	electrical resistance, Ω
R_b	ratio of beam irradiance on the tilted surface to that on the horizontal surface
r	unpolarised radiation
S	solar radiation absorbed by the solar collector, W m^{-2}
T	temperature, °C
$\dot{Q}_u$	heat flux, W
u	velocity, m/s
U, U_L	thermal transmittance, W m^{-2} K^{-1}
W	step between tubes in the solar collector, m
x	linear abscissa, m
Z	figure of merit, K^{-1}
ZT	dimensionless figure of merit

Greek symbols

α	absorbance coefficient of slab of solar collector
β	volumetric thermal expansion coefficient, K^{-1}
δ	density, kg/m^3
δ^*	solar declination, rad
ε_{pn}	difference between the Seebeck coefficients of *p*- and *n*-type elements, V/K
ϕ	latitude, rad
γ	tilt angle, rad
η_e	pump electrical efficiency
η_{fin}	fin efficiency
η_m	pump mechanical efficiency
φ, θ	angle, rad
λ	thermal conductivity, W/(m K)
μ	viscosity, Pa s
ν	kinematic viscosity, m^2/s
ρ	resistivity, Ω m
ρ_g	albedo
τ	transmittance coefficient of glass
ω	hour angle, rad
ζ	minor pressure loss coefficient
(τ_α)	transmittance-absorptance product

Sub and superscripts

φ	circumferential
b	beam
c	cold fluid
d	diffuse
e	external
h	hot fluid
i	internal
n	*n*- type thermoelement or normal direction
out	outdoor
p	*p*-type thermoelement
s	surface
sc	solar collector
x	axis direction

reservoir. Therefore they are difficult to reach, so obtaining the goal to protect them from vandalism and theft.

In this work, starting from this design hypothesis, the system is analyzed with the aim to highlight the most relevant design parameters.

Riffat and Xiaoli Ma [21] showed the convenience of thermoelectric effect in order to produce electric power and note that a thermoelectric system is adequate in cases where thermal energy is available at a low cost or free. On the other hand, they also note that these systems have a relatively low efficiency, typically around 5%. Currently many researchers are working on thermoelectric generators mainly referring to potential applications [18,20,30,11] and mathematical and physical characterization [15,10,22]. Furthermore, several research works have been focused on using solar-thermoelectric systems, also combined with photovoltaic or another technologies [17,4,31,13,29,5].

Many works in literature show how R&D focus on new materials with a higher efficiency and with a larger figure of merit [19,26,7,8,24,12].

2. The proposed model system

The proposed system is basically constituted of four sections: (1) the first section is composed of the electric user system; (2) the second section is composed of the hydraulic circuit; (3) the third section is composed of the heat exchanger of the power source (for example, solar collectors); (4) the fourth and principal section referring to the heat exchanger dipped in a cold reservoir (the heat sink), that is also the thermoelectric generator. Fig. 1 shows a simplified sketch. The electrical power produced by thermoelectric generator has to meet the requirements of the electrical load of the considered site.

For convenience, we directly report the main general relationships used in our simulation model.

The fluid speed in the circuit can be calculated by means of the mass flow rate:

$$u = 4M/\left(\delta\pi D_i^2\right) \tag{1}$$

where M is the flow rate, δ is the fluid density and D_i is the inner diameter.

The major losses are computed with the Hazen–Williams equation [2]:

$$\Delta p_{major} = 6.819L\left(\frac{u}{C_{HW}}\right)^{1.852}\left(\frac{1}{D_i}\right)^{1.167}(\delta\cdot g) \tag{2}$$

where C_{HW} is the coefficient of roughness, L is the length of the pipe, and g is the earth's standard acceleration due to gravity.

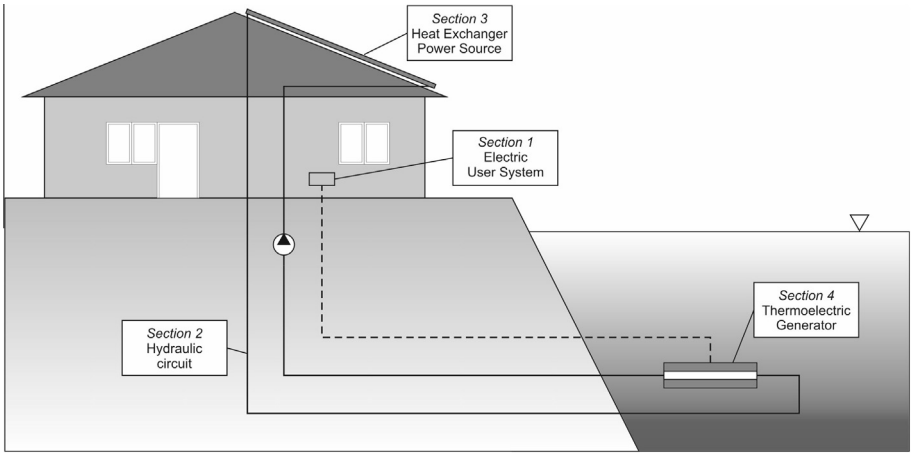

Fig. 1. A sketch of the proposed system.

The minor losses can be evaluated with reference to the particular coefficient ζ of the components that causes the pressure loss, i.e.,

$$\Delta p_{minor} = \sum_j \zeta_j \delta \frac{u^2}{2} \tag{3}$$

For the evaluation of the internal heat transfer coefficient of the tube, h_i, it is possible to use the well-known Dittus–Boelter equation [14], with the limits: $0.7 \leqslant \mathrm{Pr} \leqslant 160$; $\mathrm{Re}_D > 10{,}000$; $D/L > 10$:

$$\mathrm{Nu}_D = 0.023 \mathrm{Re}_D^{4/5} \mathrm{Pr}^z \tag{4}$$

where $z = 0.4$ for heating ($T_s > T_{fluid}$) and $z = 0.3$ for cooling ($T_s < T_{fluid}$), being T_s and T_{fluid} temperatures of the surface of the tube and of the fluid that flow through, respectively.

For the evaluation of the external heat transfer coefficient of the tube, h_e, it is possible to use the Churchill–Chu correlation [9], with the limit $10^{-5} < \mathrm{Ra}_D \leqslant 10^{12}$:

$$\mathrm{Nu}_D = \left\{ 0.60 + \frac{0.387 \mathrm{Ra}_D^{1/6}}{\left[1 + (0.559/\mathrm{Pr})^{9/16}\right]^{8/27}} \right\}^2 \tag{5}$$

In order to evaluate the dimensionless numbers, we have to compute the thermo-physical characteristics of the fluids (water) for the given value of the temperature.

The thermal conductivity λ and the density δ of the water may be evaluated utilizing the equations derived by Choi and Okos [1], under the limit $-40\ ^\circ\mathrm{C} \leqslant T \leqslant 150\ ^\circ\mathrm{C}$:

$$\lambda = 5.7109 \cdot 10^{-1} + 1.7625 \cdot 10^{-3} T - 6.7036 \cdot 10^{-6} T^2 \tag{6}$$

$$\delta = 9.9718 \cdot 10^{2} + 3.1439 \cdot 10^{-3} T - 3.7574 \cdot 10^{-3} T^2 \tag{7}$$

The specific heat c_p, the viscosity μ and the expansion coefficient β of the water are evaluated by means of the following equations, which we obtained by means of an interpolation of the related data tables [9], under limit $0\ ^\circ\mathrm{C} \leqslant T \leqslant 120\ ^\circ\mathrm{C}$:

$$c_p = 4207.7 - 1.0618T + 0.0114T^2 \tag{8}$$

$$\mu = 1.738 \cdot 10^{-3} - 5.020 \cdot 10^{-5} T + 7.961 \cdot 10^{-7} T^2 + 6.399 \cdot 10^{-9} T^3 + 1.992 \cdot 10^{-11} T^4 \tag{9}$$

$$\beta = -6.129 \cdot 10^{-5} + 1.613 \cdot 10^{-5} T - 1.594 \cdot 10^{-7} T^2 + 1.042 \cdot 10^{-9} T^3 - 2.501 \cdot 10^{-12} T^4 \tag{10}$$

The thermal diffusivity and the kinematic viscosity were calculated utilizing their definition as the function of the other computed variables.

2.1. The electrical load

The electrical load can be a generic system, for example a water pump for a well. Obviously the design of the proposed system depends on the electrical power needed by the user and by the available heat source. It is worth noting that, apart from the start-up of the system, it is a stand-alone one, it is possible to complete the plant with an array of batteries in order to compensate the lack of a power source.

2.2. The hydraulic circuit

A length of well insulated, diameter fixed copper pipe and a circulation pump constitute the hydraulic circuit. The pump sends the hot fluid through the pipe and between the two heat exchangers. As parameters, we also have the electric power of the pump and the pressure loss along the hydraulic circuit.

After setting up the geometry of the plant, it is possible to evaluate the mass flow rate of the hot fluid and then, by means of the Bernoulli equation, to compute the pressure losses.

The pump power P_w is related to the mass flow rate of the hot fluid, pressure losses and moreover with mechanical and electrical efficiencies of the pump. So we have:

$$P_w = M\Delta p/(\delta \eta_m \eta_e) \tag{11}$$

where Δp indicates the pressure losses in the whole system, the sum of major and minor losses: $\Delta p_{major} + \Delta p_{minor}$, as stated above.

2.3. The heat exchanger of the heat source

In this work we assume that the heat exchanger of the heat source is a solar collector and the main output parameters are the pressure loss of the solar collector and outlet temperature of the fluid for fixed flow rate and climatic parameters.

2.3.1. The mathematical model of the solar collector

Referring to the half width of the sheet (the length of fin) for each tube is calculated by means of the following equation:

$$l = \frac{W - D_{sc,e}}{2} \tag{12}$$

where W is the width of the step between tubes and $D_{sc,e}$ is the outer diameter of the tube in the collector.

It is now useful to introduce a parameter m that can be utilized in the following relationship:

$$m = \sqrt{\frac{U_L}{\lambda \cdot d}} \tag{13}$$

where U_L is the thermal transmittance of the solar collector, λ is the thermal conductivity of the slab and d is the thickness of the slab.

The function of the standard fin efficiency for straight fins with a rectangular profile is:

$$\eta_{fin} = \frac{\tanh(m \cdot l)}{m \cdot l} \tag{14}$$

The collector efficiency factor is provided by the following equation:

$$F' = \frac{1}{W \cdot \left(\frac{1}{D_{sc,e}+2l\eta_{fin}} + \frac{U_L}{\pi D_{sc,i} h_i}\right)} \tag{15}$$

where $D_{sc,i}$ is the inner diameter of the tube of the solar collector and h_i is the internal convective heat transfer coefficient provided by Eq. (4), where n has been fixed at the value of 0.4.

The removal factor of the solar collector is given by:

$$F_R = \frac{M \cdot c_p}{A_c \cdot U_L}\left(1 - e^{-\frac{A_c U_L F'}{M c_p}}\right) \tag{16}$$

where M is the mass flow rate, c_p is the specific heat at a constant pressure and A_c is the overall surface area of solar collectors.

The following equation provides the amount of the actual useful energy gain [6]

$$\dot{Q}_u = A_c F_R[S(\tau\alpha)_n - U_L(T_i - T_{out})]; \tag{17}$$

where S is the solar radiation absorbed by the solar collector, $(\tau\alpha)_n$ is the transmittance-absorptance product for normal direction, T_i is the inlet temperature of the hot fluid and T_{out} is the outside air temperature. The parameter S is obtained by the following equation:

$$S = I_b R_b (\tau\alpha)_b + I_d (\tau\alpha)_d \frac{1+\cos\gamma}{2} + \rho_g (I_b + I_d)(\tau\alpha)_{ground} \frac{1-\cos\gamma}{2} \tag{18}$$

where I_b and I_d are beam and diffuse components of irradiance, R_b is the ratio of beam on the tilted surface to that on the horizontal surface, γ is the tilt angle, ρ_g is the diffuse reflectance of the surroundings (albedo) and $\tau\alpha_b$, $\tau\alpha_d$ and $\tau\alpha_{ground}$ are the transmittance-absorptance products for different incident angles that are provided by Duffie and Beckman [6]. They assume the generic form:

$$(\tau\alpha) = 1.01 \cdot \tau \cdot \alpha \tag{19}$$

where τ is calculated by the following equations:

$$\tau = \exp\left(-\frac{N \cdot K_{glass} \cdot d_{glass}}{\cos\theta_2}\right) \cdot \frac{1}{2} \cdot \left(\frac{1 - r_{||}}{1 + (2N-1)r_{||}} + \frac{1 - r_{\perp}}{1 + (2N-1)r_{\perp}}\right) \tag{20}$$

where θ_2 is the angle of refraction (arcsin( ) of ratio of sin( ) of pertinent incidence angle, θ, to refractive index, n), N is the number of glass covers, K_{glass} is the extinction coefficient, d_{glass} is the thickness of the single cover, $r_{||}$ and $r_{\perp}$ are parallel and perpendicular components of the unpolarised radiation respectively:

$$r_{\perp} = \frac{\sin^2(\theta_2 - \theta)}{\sin^2(\theta_2 + \theta)} \tag{21}$$

$$r_{||} = \frac{\tan^2(\theta_2 - \theta)}{\tan^2(\theta_2 + \theta)} \tag{22}$$

The pertinent incident angle, θ, is different in the case of beam, diffuse or reflected radiation. Duffie and Beckman [6] provide the following equation to calculate these incident angles:

$$\theta_b = \arccos[\cos(\phi - \gamma)\cos\delta^* \cos\omega + \sin(\phi - \gamma)\sin\delta^*] \tag{23}$$

$$\theta_d = 59.7 - 0.1388\gamma + 0.001497\gamma^2 \tag{24}$$

$$\theta_{ground} = 90.0 - 0.5788\gamma + 0.002693\gamma^2 \tag{25}$$

Instead, the R_b coefficient is provided by the following equation:

$$R_b = \frac{\cos(\phi - \gamma)\cos\delta^* \cos\omega + \sin(\phi - \gamma)\sin\delta^*}{\cos(\phi)\cos\delta^* \cos\omega + \sin(\phi)\sin\delta^*} \tag{26}$$

where ϕ is the latitude of site, δ^* is the solar declination, ω is the hour angle.

In conclusion, the outlet temperature is provided by:

$$T_{outlet} = T_{inlet} + \frac{\dot{Q}_u}{M \cdot c_p}, \tag{27}$$

while the pressure drop caused by fluid friction is provided by Eqs. (2) and (3).

2.4. The thermoelectric generator

The model of the thermoelectric generator was fully developed by Suzuki and Tanaka [27], referring to the case of a single tube and isothermal conditions of the cold fluid.

The thermoelectric generator is the main section of the proposed system; it is made up of a heat exchanger with a set of thermocouples, dipped in the cold reservoir (the heat sink). Basically, it is represented by a cylindrical tube coated with a single layer of thermocouples (Fig. 2). It has also been assumed that the p- and n-type semiconductors are homogeneously aligned perpendicular to the heat flow, without an open space, and connected electrically in series. This is an ideal configuration of the thermoelectric generator.

The overall heat transfer coefficient U of the heat exchanger dipping in the reservoir, considering one unit of tube length, is given by:

$$U = \frac{2\pi}{\frac{1}{h_i D_i/2} + \frac{\ln(D_e/D_i)}{\lambda} + \frac{1}{h_e D_e/2}} \tag{28}$$

where λ is the thermal conductivity of thermocouples defined by:

$$\lambda = \frac{\lambda_p \varphi_p + \lambda_n \varphi_n}{\varphi_p + \varphi_n} \tag{29}$$

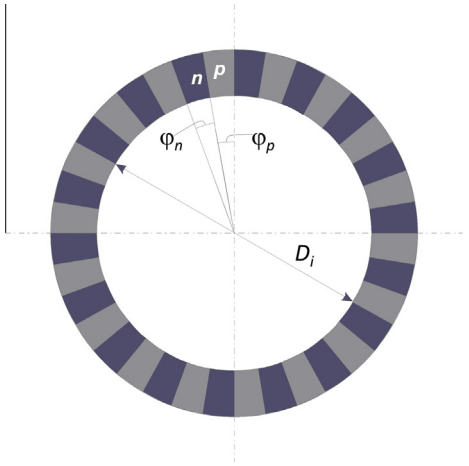

Fig. 2. A rough sketch of a section of the thermoelectric generator.

In the previous equation λ_p and λ_n are the thermal conductivity of each type of junction, and φ_p, φ_n are the angles respectively of p- and n-type semiconductors of thermocouples (Fig. 2).

Fixing a reference x on the axis of the tube and putting the 0 position at the beginning of the tube, the temperature trend of the hot fluid along the tube is given by:

$$T(x) = (T_h - T_c)e^{\left(-\frac{U}{c_p M}x\right)} + T_c \tag{30}$$

where T_h is the temperature of the hot fluid at the inlet section and T_c is the temperature of the water in the reservoir.

In order to evaluate the electrical potential difference, it is necessary to know the surface temperature of the hot and cold sides of the thermocouples, given by:

$$T_{s,h}(x) = T(x) - \frac{U}{\pi D_i h_i}(T(x) - T_c); \qquad T_{s,c}(x) = T_c + \frac{U}{\pi D_e h_e}(T(x) - T_c) \tag{31}$$

Therefore it is possible to calculate the electrical potential difference:

$$E = \left| n_\varphi n_x \varepsilon_{pn} \int_0^L [T_{s,h}(x) - T_{s,c}(x)]\mathrm{d}x \right| \tag{32}$$

where n_φ and n_x are respectively the number of thermoelectric pairs along the circumference and the number of thermoelectric pairs along the axis direction, L is the length of the thermoelectric generator.

It is necessary to consider the internal electrical resistance given by:

$$R_i = n_\varphi n_x^2 L\left(\frac{\rho_p}{\varphi_p} + \frac{\rho_n}{\varphi_n}\right)\ln\left(\frac{D_e}{D_i}\right) \tag{33}$$

The output electrical power, optimized by balancing the internal and external resistances, is given by:

$$P = \frac{E^2}{4R_i} = \frac{n_\varphi n_x [Mc_p \varepsilon_{pn}(T_h - T_c)]^2}{16(R_p + R_n)L}\left\{\frac{\ln(D_e/D_i)}{\pi\lambda}\left[1 - e^{\left(-\frac{UL}{Mc_p}\right)}\right]\right\}^2 \tag{34}$$

where R_p and R_n are respectively the resistance of p- and n-type elements.

$$R_p = \rho_p \frac{n_x}{\varphi_p}\ln\left(\frac{D_e}{D_i}\right); \quad R_n = \rho_n \frac{n_x}{\varphi_n}\ln\left(\frac{D_e}{D_i}\right) \tag{35}$$

The end of maximizing the output power has been achieved by adopting the following angles of p- and n-type elements:

$$\varphi_p = \frac{2\pi\sqrt{\lambda_n\rho_p}}{n_\varphi(\sqrt{\lambda_n\rho_p} + \sqrt{\lambda_p\rho_n})}; \quad \varphi_n = \frac{2\pi\sqrt{\lambda_p\rho_n}}{n_\varphi(\sqrt{\lambda_n\rho_p} + \sqrt{\lambda_p\rho_n})} \tag{36}$$

3. Simulation

With the aim to evaluate the performances of the proposed system, the authors have built a simulating software, in C-language, that utilizes the above mathematical model. Some input values regarding the thermoelectric generator were taken from Suzuki and Tanaka [27]. In order to assess the electrical yearly energy production, meteorological data of a whole year were utilized as input data in order to evaluate the thermal production of the solar collectors.

The simulation of the performances of the system has been conducted in a quasi-steady state regime. This choice directly depends on the structure of the proposed model that describes the thermophysical behaviour of the system in a time-invariant way. This allows to lead to a numeric step by step simulation where, in each analyzed step, the system should reach its regime conditions. Due to the structure of the working cycle and depending on the fluid circulating through it, the time step selected for the simulation was an hour. The kind of climatic data set utilized as an input for the simulation is the Test Referee Years (TRY), which provides hourly values of climatic parameters of the selected sites. If TRY is not available, it is possible to use a reduced weather dataset [3].

The utilized climatic database is the Test Reference Year for the city of Palermo, Italy [25]; Figs. 3 and 4 show daily trends of air temperature and solar radiation respectively. Other input values were taken from technical and commercial literatures.

3.1. Values of parameters used in the simulation

It was assumed that the collectors were installed in the city of Palermo (38.12N, 13.34E – South of Italy), oriented South, with a tilt angle equal to 30°, and the albedo of the surrounding area was equal to 0.2.

The main characteristics of the solar collector are reported in Table 1, while Tables 2 and 3 report the main parameters of thermoelectric elements and thermoelectric generator respectively. The figure of merit of the thermoelectric module, Z, is $2.59\ 10^{-3}\ K^{-1}$.

The number of thermocouples, n_φ, in a circular section is calculated by considering a constraining of the minimum width of 6 mm for each thermocouple.

The main parameters of the thermo-hydraulic circuit used are reported in Table 4.

4. Results and discussion

After setting the above system parameters, running the simulating software provides the yearly data output. The software gives as output the net electrical energy production, the efficiency of the

Fig. 3. The trend of max and min daily air temperature of Palermo's TRY.

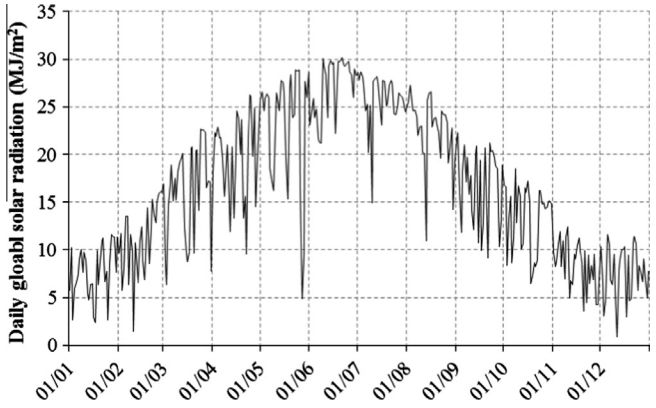

Fig. 4. The trend of daily global solar radiation of Palermo's TRY.

Table 1
Main characterizing values of the solar collector.

Parameter	Value
Surface, A_c (*variable parameter*)	2–20 m^2
Overall loss coefficient, U_L	8.0 W m^{-2} K^{-1}
Number of glass covers, N	1
Thickness of glass, d_{glass}	2.3 mm
Extinction coefficient, K_{glass}	16.1
Cover refractive index, n	1.526
Transmittance-absorptance product, $(\tau\alpha)$	0.826 584
Riser tube spacing, W	0.15 m
Riser tube number	5
Length of each tube	2 m
Outer diameter of the riser tube, $D_{sc,e}$	10 mm
Inner diameter of the riser tube, $D_{sc,i}$	9.6 mm
Absorber sheet thickness, d	0.5 mm
Thermal conductivity, λ	385 W m^{-1} K^{-1}

Table 2
Characterizing values of the thermoelectric elements.

Thermoelectric element	Absolute Seebeck coefficient ε (μV K^{-1})	Electric resistivity ρ ($\mu\Omega$ m)	Thermal conductivity λ (W m^{-1} K^{-1})
p-Type element Bi-54.3 at.% Te	162	5.55	2.06
n-Type element Bi-64.5 at.% Te	−240	10.1	2.02

Table 3
Characterizing values of the thermoelectric generator.

Section	Parameter	Value
Thermoelectric device	Length, L	10 m
	Thickness of thermocouples	0.02 m
	Number density of thermocouples, n_x	50 m^{-1}
	Inner diameter, D_i (*variable parameter*)	9.6, 14.0, 18.0, 23.2, 29.0, 36.20, 45.80 mm
Cold fluid (Water)	Temperature, T_c	15 °C

Table 4
Characterizing values of the thermo-hydraulic circuit.

Section	Parameter	Value
Pipe	Type of tube	DN90, PE80-PFA8
	Length of pipe	40 m
	Coefficient of roughness, C_{HW}	150
	Inner diameter, D_i (*variable parameter*)	9.6, 14.0, 18.0, 23.2, 29.0, 36.20, 45.80 mm
Working fluid	Speed, u (*variable parameter*)	0.3–2.3 m/s
Pump	Electrical efficiency, η_e	95%
	Mechanical efficiency, η_m	80%

whole system, the heat exchanged by the thermoelectric generator and the sink, and the electrical power produced. This provides the average, minimum and maximum values of the above parameters. The net electrical power is defined as the electrical power production (see Eq. (34)) minus the pumping power consumption (see Eq. (11)).

Each of these values was computed varying the working fluid velocity, the pipe diameter (both thermoelectric generator and hydraulic circuit) and the surface of the solar collector system.

Fig. 5 shows that, in the range of the speed considered in the simulations (0.3–2.3 m/s), the trend of the net electrical production has a maximum for each diameter. Moreover, the number of curves that show a maximum value seems to increase with the increasing of the collector surface, and the maximum occurs for the lower speed of the working fluid when the diameter increases. Furthermore, the optimal value of the working fluid speed is around 0.8 m/s. In the case of high diameters, the system is oversized and requires a larger collector surface, so hereinafter we refer only to the 9.6 mm diameter, because it appears to be in compliance with the aim of the application of the case study.

The plots of the Net Energy Output varying the speed of working fluid are reported in Fig. 6, for selected solar collector surfaces. As expected, the diagram shows that, increasing the solar collector surface, Net Output Energy grows. It also highlights that there is a maximum for each curve and that, increasing the solar collector surface, the maximum value occurs for a slightly higher speed.

Similarly in Fig. 7 the maximum efficiency of the whole system has the same behaviour. The more the solar collector surface increases, the more the maximum efficiency of the whole system grows. The increment of the system's maximum efficiency decreases with the growing of the solar collector surface (lines are closer increasing collector surface). For a lower value of the working fluid speed, Fig. 7 also shows that it is possible to achieve a better efficiency with a smaller solar collector surface.

Fig. 8 shows that the maximum electrical power of the system has similar behaviour to that of the maximum efficiency with the difference that, increasing the speed values, the slope of the curves decreases.

The maximum temperature drop of the working fluid decreases exponentially with the increasing of the working fluid speed and, considering the corresponding increasing of the solar collector surface, the starting slope of curve is more accentuated, as shown in Fig. 9.

In Fig. 10 the trend of the daily mean temperature difference between the two sides of the TE generator are reported in the year for three different speeds, for $D_i = 9.6$ mm and $A_c = 8$ m^2. These plots, especially for the lower speeds, reflects the trend of daily global solar radiation: values oscillate with an amplitude that amounts to 15 °C for the lowest speed of 0.3 m/s, to a value of 5 °C for the highest speed of 2.3.

It is also possible to see that, increasing the speed value of the circulating fluid, curves run with a higher value of temperature. From a mean ΔT of around 12.5–20 °C for $u = 0.3$, in the case of $u = 2.3$ the mean value is around 40 °C. Moreover the dimensionless figure of merit, ZT, varies from 0.750 to 0.826.

In Fig. 11 the temperature difference between the two sides of the TE module versus hourly outside air temperature are reported, for $D_i = 9.6$ mm and $A_c = 8$ m^2. Basically it is possible to see that the values of outside air temperature are concentrated in the range of 10–30 °C and that there is no particular dependence between the two parameters. It is noteworthy that increasing speed, as stated in Fig. 11a–c, the minimum values of $\Delta T_{\text{cold-hot}}$ occur for the higher temperature. This is due to higher losses that do not permit the imposed self-reliance of the system. Furthermore, the higher values of $\Delta T_{\text{cold-hot}}$ occur for the higher speed of working fluid.

Fig. 12 shows that the temperature difference between the two sides of the TE modules depend on global solar radiation, for $D_i = 9.6$ mm and $A_c = 8$ m^2. The more global solar radiation increases, the more the temperature difference between the two sides of the TE modules increases. The same remarks relating to minimum and higher values of $\Delta T_{\text{cold-hot}}$ may be repeated.

Fig. 13 illustrates the power trend of the hydraulic pump vs speed of the working fluid as a function of the inner diameter as well as of the surface area of the solar collector. As expected, the power of the hydraulic pump increases with increasing of speed of the working fluid (see Eqs. 2, 3 and 11), of the inner diameter (see Eqs. 1, 2 and 11) as well as of the surface area of the solar collector (obviously major and minor losses increase).

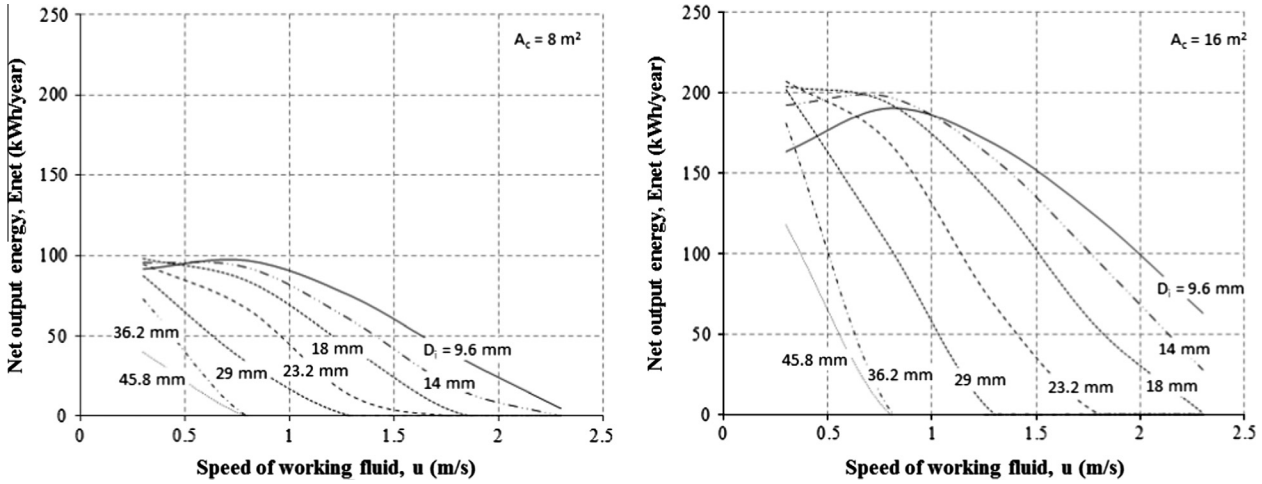

Fig. 5. Net electrical energy production of the whole system in the case of collector surface equal to 8 cm^2 and 16 m^2, for various diameters of the tube.

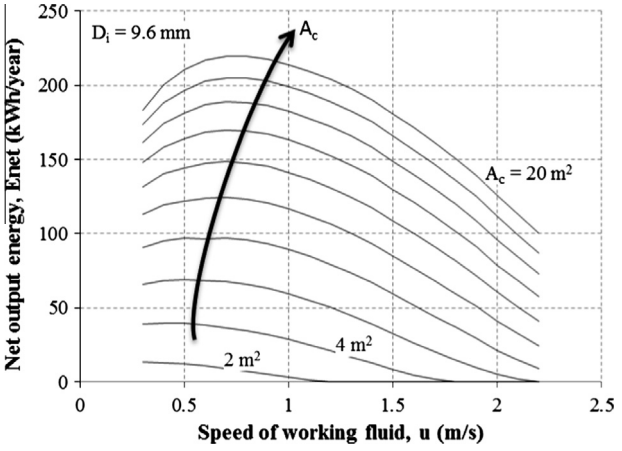

Fig. 6. Net electrical energy production of the whole system in the case of D_i = 9.6 mm, by varying the collector surface.

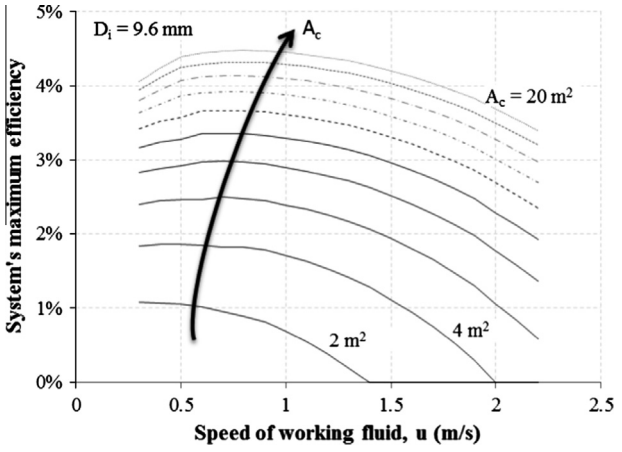

Fig. 7. Maximum efficiency of the whole system in the case of D_i = 9.6 mm, by varying the collector surface.

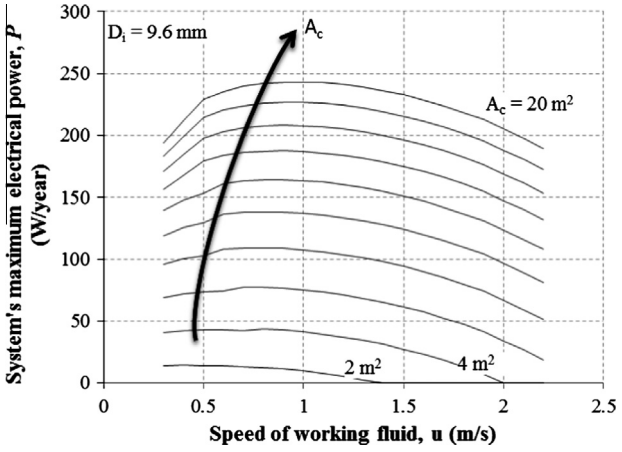

Fig. 8. System's maximum electrical power in the case of D_i = 9.6 mm varying the collector surface.

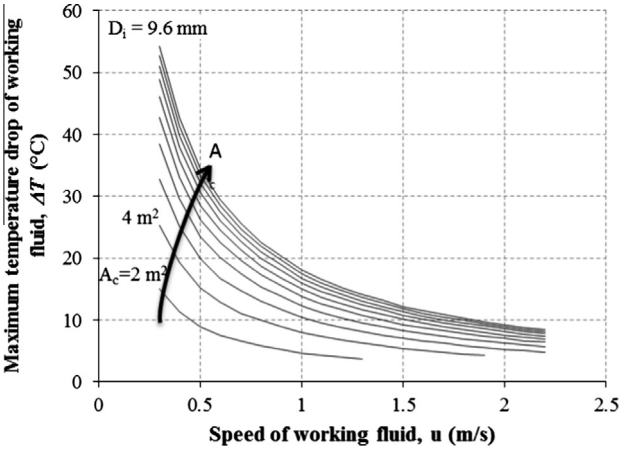

Fig. 9. Maximum temperature difference of working fluid in the case of D_i = 9.6 mm, by varying the collector surface.

In order to assess the magnitude of the economic feasibility of the proposed system utilizing the Peltier cells, a rough estimate cost per unit of energy produced was performed.

The cost of a single thermocouple was estimated at around 0.22 €/thermocouple considering a mean current commercial cost of available thermoelectric modules. The cost of a thermal solar collector was estimated at around 800 €/m^2 on mean market prices. The overall cost of the pipes and hydraulic components was estimated at around 500 € on mean market. Considering the

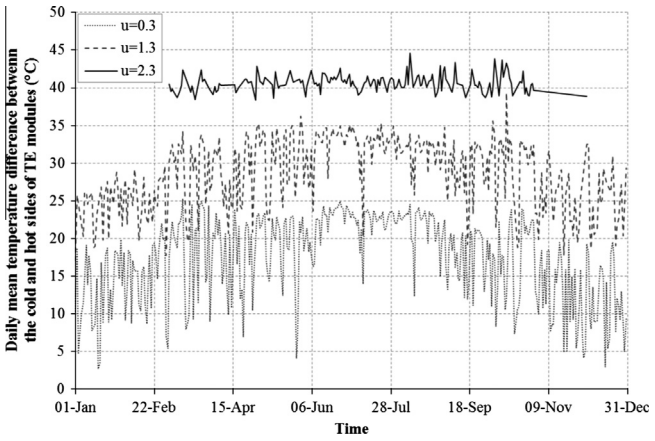

Fig. 10. The trend of temperature difference between two sides of the TE modules, for D_i = 9.6 mm and A_c = 8 m^2.

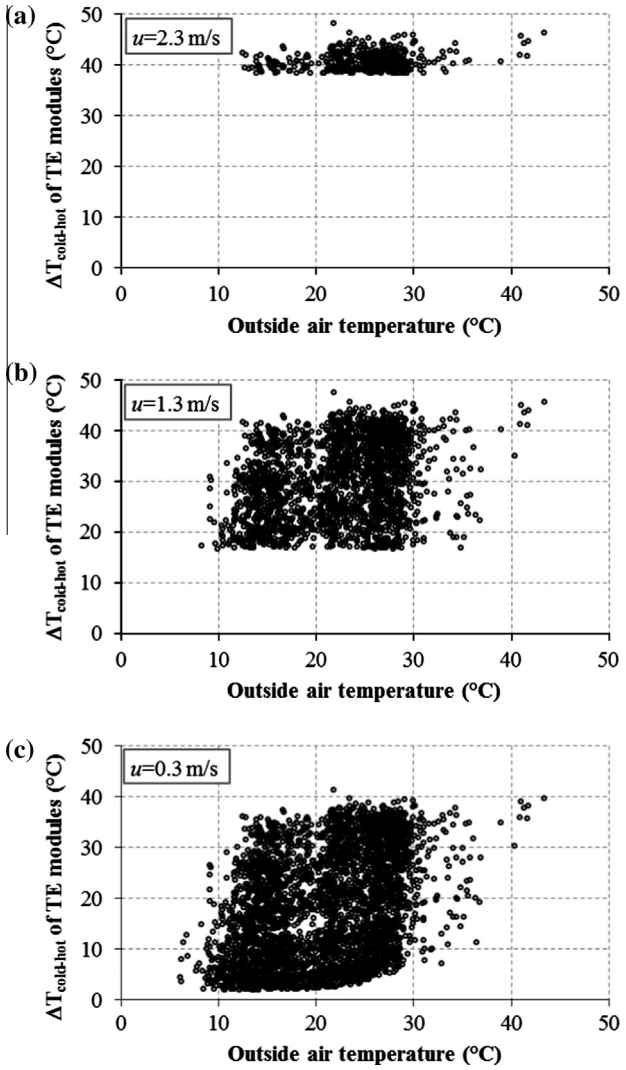

Fig. 11. The temperature difference between two sides of the TE modules versus hourly outside air temperature (for three different values of speed: a. u = 2.3, b. u = 1.3, c. u = 0.3), for D_i = 9.6 mm and A_c = 8 m^2.

case of a total thermal collector surface equal to 16 m^2, a pipe with the inner diameter of 14 mm, therefore 7000 thermocouples for 10 m of length of thermoelectric device, a working fluid speed of 0.8 m/s, we roughly obtained an installation cost of around

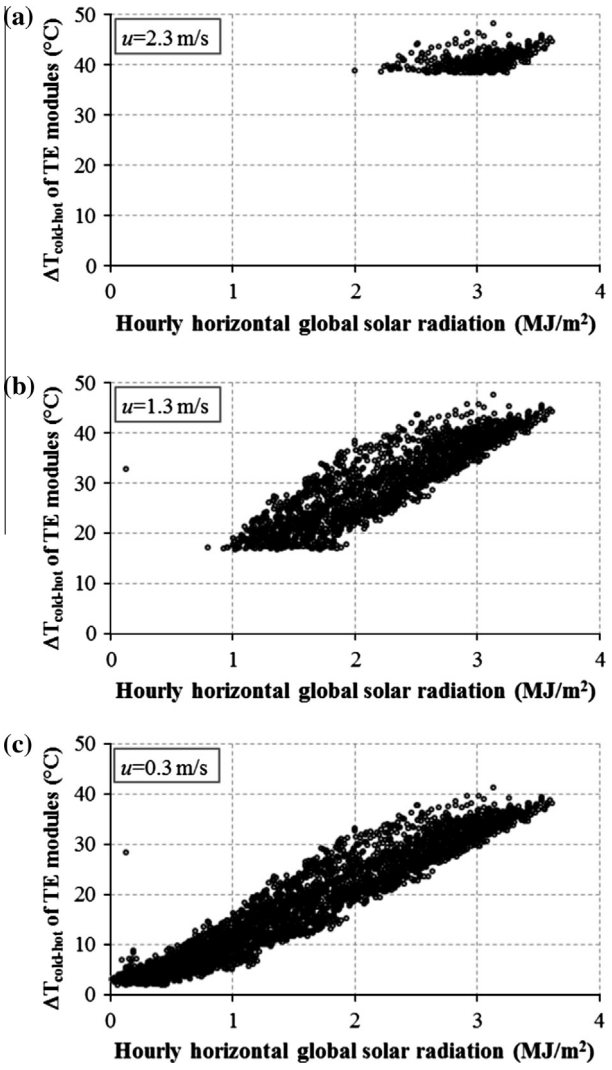

Fig. 12. The temperature difference between two sides of the TE modules versus hourly global solar radiation (for three different values of speed: a. u = 2.3, b. u = 1.3, c. u = 0.3), for D_i = 9.6 mm and A_c = 8 m^2.

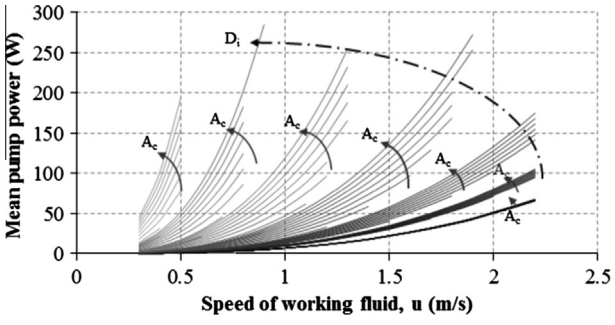

Fig. 13. Trend of hydraulic pump power.

$800 \times 16 + 0.22 \times 7\ 000 + 500 = 14\ 840.00$ € with an annual net energy production of 197.27 kW h/a. Considering a system lifetime of 25 years, we get a cost of 3.01 €/kW h.

This cost is quite expensive compared to the corresponding cost of the photovoltaic system. Indeed, considering a PV-system, we have a mean installation cost of around 2000 €/kW p and the related expected energy production in the South of Italy is at around 1500 kW h/a. Considering a system lifetime of 25 years, we evaluated a cost of 0.05 €/kW h, a value 56 times less than the proposed system.

5. Conclusions

The proposed system utilizes the thermal difference between a lower temperature sink and a higher temperature source. The system is focused on the thermoelectric generator, basically a heat exchanger composed of a set of thermocouples. The main parameters of the system are the thermal power and the temperature of the heat source. Considering these parameters and other characteristic variables, simulating software was developed by the authors to perform several tests.

Results show that, with reference to the annual energy production, an optimization of the system is possible choosing a suitable set of design parameters, basically: an inner diameter, a solar collector surface and a working fluid speed. As expected, the outcomes also point out that the size of the inner diameter of proposed system depends on amount of available heat flux and that the efficiency of the proposed system is less than 5%, considering the actual material thermocouples.

The complexity and the poor efficiency of the proposed system, as well as the high cost of materials, discourages this type of application of thermoelectric generators.

However, the results obtained suggest further investigation on newer thermoelement materials in order to achieve higher efficiency and lower costs.

References

[1] ASHRAE. ASHRAE handbook – refrigeration. Atlanta, USA: American Society of Heating, Refrigerating and Air-Conditioning Engineers Inc.; 2006.

[2] ASHRAE. ASHRAE handbook – fundamentals. Atlanta, USA: American Society of Heating, Refrigerating and Air-Conditioning Engineers Inc.; 2009.

[3] Cannistraro G, Giaconia C, Pietrafesa M, Rizzo G. Reduced weather data for building climatization and application to 29 European locations. Energy 1995;20(7):637–46.

[4] Chávez-Urbiola EA, Vorobiev YV, Bulat LP. Solar hybrid systems with thermoelectric generators. Sol Energy 2012;86:369–78.

[5] Chen G. Theoretical efficiency of solar thermoelectric energy generators. J Appl Phys 2011;109. pp. 104908-1–8.

[6] Duffie JA, Beckman WA. Solar engineering of thermal processes. 3rd ed. Hoboken, New Jersey, USA: John Wiley & Sons Inc.; 2006.

[7] Eidelman ED, Ya Vul' A. The strong thermoelectric effect in nanocarbon generated by the ballistic phonon drag of electrons. J Phys: Condens Matter 2007;19(266210):1–12.

[8] Hiroshige Y, Ookawa M, Toshima N. Thermoelectric figure-of-merit of iodine-doped copolymer of phenylenevinylene with dialkoxyphenylenevinylene. Synth Met 2007;157:467–74.

[9] Incropera FP, DeWitt DP. Fundamentals of heat and mass transfer. 4th ed. New York: John Wiley & Sons; 1996.

[10] Karabetoglu S, Sisman A, Ozturk ZF, Sahin T. Characterization of a thermoelectric generator at low temperatures. Energy Convers Manage 2012;62:47–50.

[11] Karri MA, Thacher EF, Helenbrook BT. Exhaust energy conversion by thermoelectric generator: two case studies. Energy Convers Manage 2011; 52(3):1596–611.

[12] Kiriharaa K, Nagatac T, Kimurab K. Thermoelectric properties of AlPdRe icosahedral alloys. J Alloy Compd 2002;342:469–72.

[13] Kraemer D, Poudel B, Chen G. High-performance flat-panel solar thermoelectric generators with high thermal concentration. Nat Mater 2011; 10:532–8.

[14] Kreith F, editor. The CRC handbook of thermal engineering. Boca Raton: CRC Press; 2000.

[15] Lesage FJ, Sempels ÉV, Lalande-Bertrand N. A study on heat transfer enhancement using flow channel inserts for thermoelectric power generation. Energy Convers Manage 2013;75:532–41.

[16] Morale M, Rodonò G, Scaccianoce G, Tucciarelli T, 2009. Electric energy production from thermal energy: combined use of solar radiation and water reservoirs. In: Proc. of energy, environment and water desalination conference; Tripoli.

[17] Najafi H, Woodbury KA. Modeling and analysis of a combined photovoltaic-thermoelectric power generation system. J Solar Energy Eng 2013;135. pp. 031013-1–8.

[18] Najafi H, Woodbury K. Optimization of a cooling system based on Peltier effect for photovoltaic cells. Sol Energy 2013;91:152–60.

[19] Noudem JG, Lemonnier S, Prevel M, Reddy ES, Guilmeau E, Goupil C. Thermoelectric ceramics for generators. J Eur Ceram Soc 2008;28:41–8.

[20] Rahbar N, Esfahani JA. Experimental study of a novel portable solar still by utilizing the heatpipe and thermoelectric module. Desalination 2012;284: 55–61.

[21] Riffat SB, Ma Xiaoli. Thermoelectrics: a review of present and potential applications. Appl Therm Eng 2003;23:913–35.

[22] Rodríguez A, Vián JG, Astrain D, Martínez A. Study of thermoelectric systems applied to electric power generation. Energy Convers Manage 2009;50(5):1236–43.

[23] Rowe DM. CRC handbook of thermoelectrics. Florida, USA: CRC Press; Boca Raton; 1995.

[24] Simkin BA, Hayashi Y, Inui H. Directional thermoelectric properties of Ru_2Si_3. Intermetallics 2005;13:1225–32.

[25] Sorrentino G, Scaccianoce G, Morale M, Franzitta V. The importance of reliable climatic data in the energy evaluation. Energy 2012;48(1):74–9.

[26] Sudhakar Reddy E, Noudem JG, Goupil C. Open porous foam oxide thermoelectric elements for hot gases and liquid environments. Energy Convers Manage 2007;48:1251–4.

[27] Suzuki OR, Tanaka D. Mathematic simulation on thermoelectric power generation with cylindrical multi-tubes. J Power Sources 2003;124:293–8.

[28] United Nations. Kyoto protocol to the United Nations framework convention on climate change. Kyoto, Japan; 11 December, 1997 [Entered into force on 16 February 2005].

[29] Van Sark WGJHM. Feasibility of photovoltaic-thermoelectric hybrid modules. Appl Energy 2011;88:2785–90.

[30] Whalen SA, Dykhuizen RC. Thermoelectric energy harvesting from diurnal heat flow in the upper soil layer. Energy Convers Manage 2012;64:397–402.

[31] Xiao J, Yang T, Li P, Zhai P, Zhang Q. Thermal design and management for performance optimization of solar thermoelectric generator. Appl Energy 2012;93:33–8.